**Wind and Structures**, *Vol. 24, No. 5 (2017) 481-500*
DOI: https://doi.org/10.12989/was.2017.24.5.481 

# A 3-DOF forced vibration system for time-domain aeroelastic parameter identification

Heather Scot Sauder[1,2a] and Partha P. Sarkar[*2]

[1]*CPP Wind Engineering, Fort Collins, CO 80525, USA*
[2]*Department of Aerospace Engineering, Iowa State University, Ames, IA 50011, USA*

*(Received November 20, 2016, Revised April 25, 2017, Accepted May 7, 2017)*

**Abstract.** A novel three-degree-of-freedom (DOF) forced vibration system has been developed for identification of aeroelastic (self-excited) load parameters used in time-domain response analysis of wind-excited flexible structures. This system is capable of forcing sinusoidal motions on a section model of a structure that is used in wind tunnel aeroelastic studies along all three degrees of freedom - along-wind, cross-wind, and torsional - simultaneously or in any combination thereof. It utilizes three linear actuators to force vibrations at a consistent frequency but varying amplitudes between the three. This system was designed to identify all the parameters, namely, aeroelastic- damping and stiffness that appear in self-excited (motion-dependent) load formulation either in time-domain (rational functions) or frequency-domain (flutter derivatives). Relatively large displacements (at low frequencies) can be generated by the system, if required. Results from three experiments, airfoil, streamlined bridge deck and a bluff-shaped bridge deck, are presented to demonstrate the functionality and robustness of the system and its applicability to multiple cross-section types. The system will allow routine identification of aeroelastic parameters through wind tunnel tests that can be used to predict response of flexible structures in extreme and transient wind conditions.

**Keywords:** flutter; parameter identification; time-domain, wind tunnel tests, forced vibration system

## 1. Introduction

The complex interaction between the wind and a structure induces specific wind loads on the structure that are capable of producing large amplitude motions which may be catastrophic. Aeroelasticity is the study of the significant interaction of aerodynamic forces with the elastic response of a flexible structure. Major wind-induced instabilities can be generally classified as: self-excited (motion-induced), self-excited in the presence of buffeting, and vortex-induced. The combined effect of the three loads depict the response of a specific structure in any given wind condition. Self-excited loads are the product of the motion of a structure as it perturbs the flow around it such that the modified flow pattern produces additional aerodynamic damping and stiffness loads. If the structure is given an initial deflection, its motion will either decay or increase which is dependent on whether the wind is transferring energy to the structure or helping to

*Corresponding author, Professor, E-mail: ppsarkar@iastate.edu
[a] Formerly Graduate Research Assistant


http://www.techno-press.org/?journal=was&subpage=8 ISSN: 1226-6116 (Print), 1598-6225 (Online)

dissipate the kinetic energy of the structure. The theoretical dividing line between the decay and the increase is identified as the critical flutter speed. Buffeting wind loads are fluctuating loads acting on a structure and are induced by upstream wind turbulence and structure-induced turbulence. The fluctuating wind loads can be calculated based on the statistical description of the turbulence characteristics of the undisturbed flow approaching the structure and the signature turbulence due to the structure. Aerodynamic admittance function formulation, proposed by Davenport (1962), can be used to convert the wind turbulence characteristics into wind loads on the structure in frequency domain. Vortex-induced loads cause large amplitude vibrations over a specific range of wind speeds or "lock-in" wind speed. Vortices that shed from opposite surfaces of a structure alternately result in dynamic pressure distributions producing cross-wind vibration of the structure. The "lock-in" wind speed for vortex-induced vibrations is determined from the Strouhal Number (St) for the given cross-sectional shape, Strouhal (1878), and the amplitude of the vibration can be determined from the Scruton Number (Sc), Scruton (1981), for the structure.

These wind induced loads play a major role in the design of flexible structures such as wind turbine blades, long-span bridges, high-mast poles and tall buildings. The complexity of the fluid-structure interaction makes analytical and computational simulations challenging. Therefore, to capture the complexities of the flow around a vibrating body it is necessary to perform wind tunnel tests. Three commonly used wind tunnel tests to extract the information on the aeroelastic behavior of models are scaled models of the full structure, taut-strip models, and section models. Scanlan and Tomko (1971) first introduced the method of extracting flutter derivatives from section model wind tunnel tests while Davenport *et al.* (1971) used a taut-strip method. Comparison between the two methods was done by Scanlan *et al.* (1997). This work uses sections models so a brief overview of section model methods follows.

A section model is a scaled and rigid geometrically faithful model of a two-dimensional cross-section of a body. Section model is commonly used to determine the aeroelastic load functions for a particular prototype body with a specific cross-sectional shape. End plates are typically used to reduce the aerodynamic end effects on the model and essentially ensure a two-dimensional flow over the cross-section. The aeroelastic load functions extracted from wind tunnel tests are extended to predict the response of the prototype structure.

Scanlan and Tomko (1971) developed the self-excited load formulation in frequency domain in terms of flutter derivatives. Wind tunnel tests to extract flutter derivatives typically use a free vibration type test with varying degrees-of-freedom included depending on the cross-section. Free vibration tests involve giving the model a constant initial displacement and measuring the model's displacement time history at several wind speeds. In order to extract all 18 flutter derivatives Sarkar *et al*. (2004) designed a three-degree-of-freedom (DOF) elastic suspension system that was suitable for free vibration. Several other wind tunnel free vibration rigs have been developed with all three DOFs, Dallaire *et al.* (2016) and Prud'homme *et al.* (2015). However, these systems have their limitations. First, free vibration tests do not allow for testing at high wind speeds due to the probability of either onset of divergent response (flutter) in some cross sections or highly decayed response because of high aeroelastic damping that occur in most cross sections. Second, limitation in the amplitude of vibration in the along-wind direction at high wind speeds due to a large mean drag force acting on the model and hence a large mean displacement that would significantly affect the 3-DOF results, specifically seen in the system designed by Sarkar *et al.* (2004). Third, the flutter derivatives that are meant to be strictly valid for small amplitudes of the structure are found to be sensitive to amplitudes for some cross sections, whereas it is difficult to maintain consistent amplitudes at all wind speeds in these free-vibration systems. These

limitations and the benefits of time-domain analysis prompted the development of forced vibration methods to extract the aeroelastic load functions.

Time-domain methods for self-excited loads are more applicable to finite element modeling, transient wind response, feed-back based control strategies, and fatigue life estimations. A method based on the Rational Function Approximation developed by Roger (1977) using a *two-degree-of-freedom* (vertical and torsional) forced vibration system was developed by Cao and Sarkar (2012). This method directly extracted the rational functions by measuring model displacement and surface pressure. The system developed for these forced vibration tests consisted of two motors mounted outside the wind tunnel and connected into the elastic suspension system designed by Sarkar *et al.* (2004) to create simultaneous or independent cross-wind and torsional vibrations at several frequencies and amplitudes. Other forced vibration rigs have been developed but are limited to the same degree-of-freedom combination and do not allow for the coupled motion, Permata *et al.* (2013). For some cross-sections, particularly more bluff ones, it is necessary to include the along-wind loads and displacements in the analysis of the self-excited excitation which prompted the development of a forced vibration system that could create simultaneous or independent cross-wind, along-wind and torsional vibrations. Additionally, for the analysis of more complex structures, like a wind turbine blade, where the response of the entire blade is highly coupled between all three-degrees-of-freedom a full analysis is exceedingly important.

This work describes a prototype three-degree-of-freedom forced vibration system that was designed, built and demonstrated in the Wind Simulation and Testing Laboratory at Iowa State University. The system will allow routine identification of aeroelastic parameters through wind tunnel tests in the future that can be used to predict response of flexible structures in extreme and transient wind conditions. Results from three experiments, airfoil, streamlined bridge deck and a bluff-shaped rectangular section, are presented to demonstrate the functionality and robustness of the system and its applicability to multiple cross-section types. Rational function coefficients of these sections are presented here and converted to their flutter derivative counterpart for comparison with previous results for validation.

## 2. Component description and assembly of system

The components that were used to assemble the three-DOF forced vibration system are described here. This system enables simultaneous or independent cross-wind, along-wind and torsional motions of a cantilevered section model. It is capable of capturing the effects of aeroelastic coupling between different degrees of freedom of a section model subjected to wind loading.

The system was designed as a set of 3 nested frames fixed within a stationary frame. There are 2 dynamic frames, each of which slide along 2 polished rods, one for the along-wind component and the other for the cross-wind component of the motions. The frame for the cross-wind component is mounted with the one for along-wind component and the frame for the torsional component is installed within the innermost cross-wind component frame. Fig. 1 shows the entire system mounted under the wind tunnel floor. The component for each degree of freedom will be described in the subsequent sections.

### 2.1 Cross-wind and along-wind degrees-of-freedom

Fig. 2 shows the 3DOF system mounted under the wind tunnel from underneath and a side view. The two linear systems (along-wind and cross-wind) were built using four linear bearings each (*McMaster Carr, Inc*, part number 9338T100) mounted on polished steel rods. The 2 rods for the along-wind section are connected into a stationary frame made of aluminum T-slotted framing which is mounted underneath the floor of the wind tunnel. The friction in the bearings was not a concern because the frame is being forced to vibrate at a specific frequency and amplitude. The motors for the two linear systems were Deluxe Rod Actuators (*Firgelli Automations*) with a 0.15 m (6 in) stroke length. These 12 VDC actuators have a maximum speed of 0.08 m/s (3 in/s) with 0.44 kN (100 lbs) of force. The stroke length was chosen to allow a maximum amplitude of 0.05 m (2 in) to enable high-amplitude vibrations to study their effects if necessary.

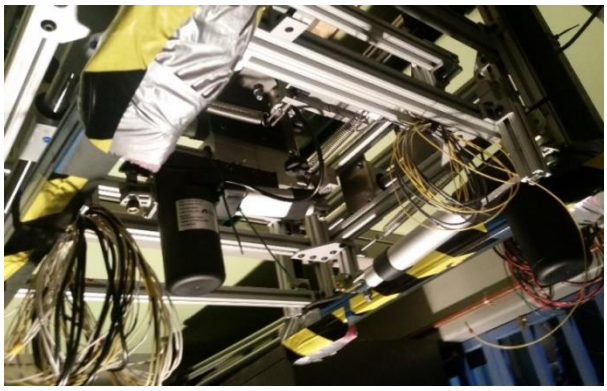

Fig. 1 3-DOF forced vibration system under the floor of the wind tunnel.

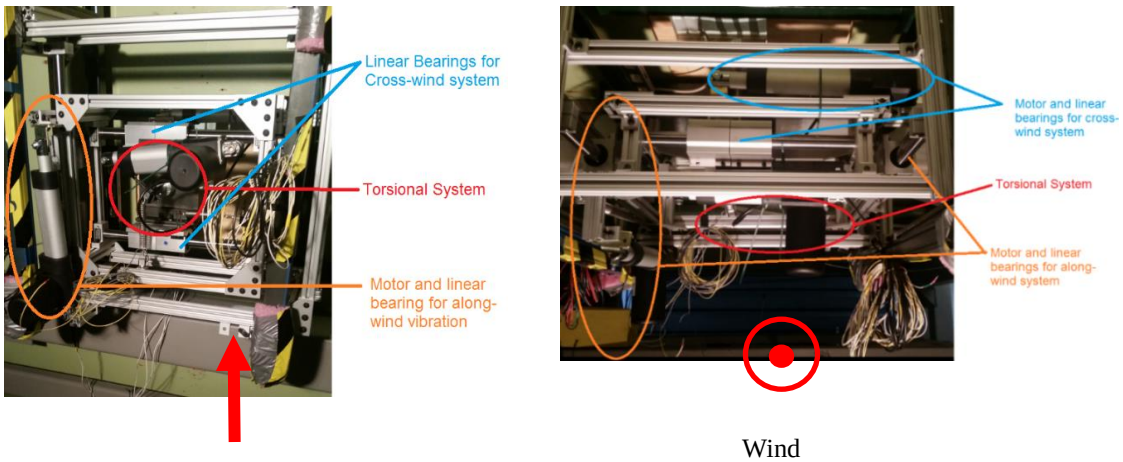


(a) View from under the wind tunnel with wind direction denoted

(b) Downwind view with wind coming out of the page

Fig. 2 3-DOF Forced vibration system mounted under the aerodynamic test section

(a)

(b)

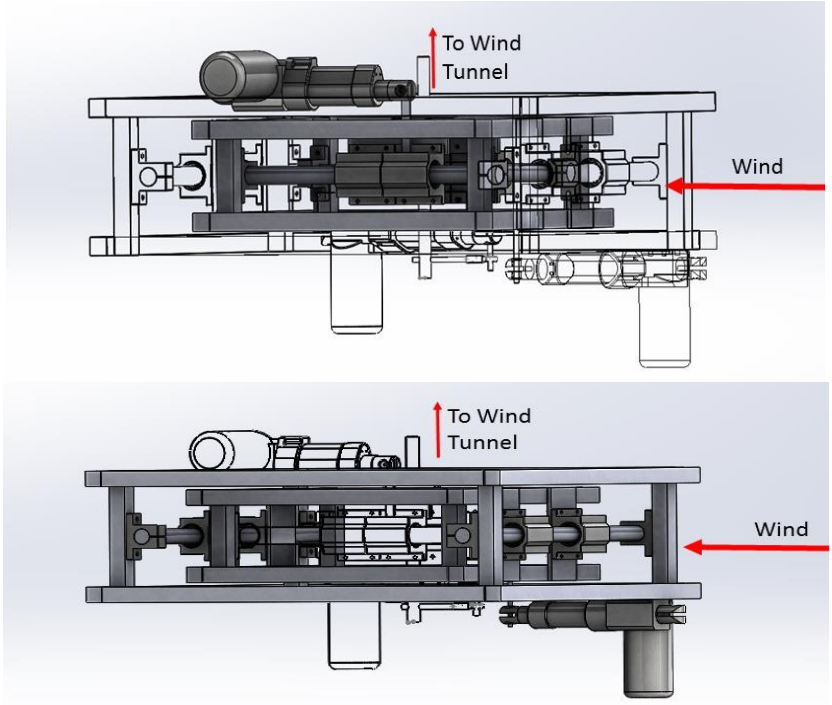


Fig. 3 SolidWorks model of the 3DOF forced vibration system. (a) interior cross-wind dynamic frame mounted inside the along-wind frame, and (b) the along-wind frame mounted inside the stationary outer frame

Fig. 3 shows the SolidWorks schematic for the two linear dynamic systems. On the design in (a) shows the exterior stationary frame with the along-wind dynamic frame mounted inside it. The image in (b) shows the cross-wind frame installed inside the along-wind component. In an effort to clarify the images several components are hidden from view or are shown as wire frames.

### *2.2 Torsional degree-of-freedom assembly*

The torsional assembly was designed to convert linear motion from an actuator into rotational motion. Fig. 4 shows a SolidWorks schematic of the design of the torsional system. A ball bearing (*McMaster Carr*, part number 6494K38) was mounted into the system that was vibrating in the cross- and along-wind directions. A solid steel rod runs through the bearing and connects perpendicularly into the motor. A Deluxe Rod Actuator (*Firgelli Automations*) with a 0.08 m (3 in) stroke length was used for the torsional system. This system has a maximum amplitude of 10 degrees, allowing high-amplitude vibration in the rotational direction if necessary.

### *2.3 Control system*

A control system was designed for this system to allow independent amplitude of vibration along each degree of freedom (DOF) but with the same frequency. Although maintaining an

identical frequency along all 3DOF is desirable for maintaining consistency between the three subsets of identified parameters associated with each degree of freedom, in the future, the control system could be modified if necessary to allow for independent frequencies using a parallel computing method. An Arduino Uno R3 board was used to communicate between the motors and the computer.An Adafruit Motor/Stepper/Servo Shield for Arduino v2.3 was used for communicating with the three motors through the Pulse Width Modulation (PWM) ports on the Arduino. The Motor shield allows for up to four DC motors to be connected at the same time and the shield can be stacked to connect more motors to the system. The motors required 12V DC and a higher current than the motor shield could supply, therefore, three IBT-2 motor drivers were used to connect the motors to the system and an AC 110V/220V to DC 12V 33A Switch Power Supply Driver was used to supply power to the three motors. The PWM signal would pass from the Arduino into the motor shield which would then communicate with the PWM chips in the IBT-2 which would direct the correct voltage pulses into the motors. Fig. 5 shows the interior of the control box developed. MATLAB Arduino toolkit was used to program the motors to vibrate in a sinusoidal fashion.

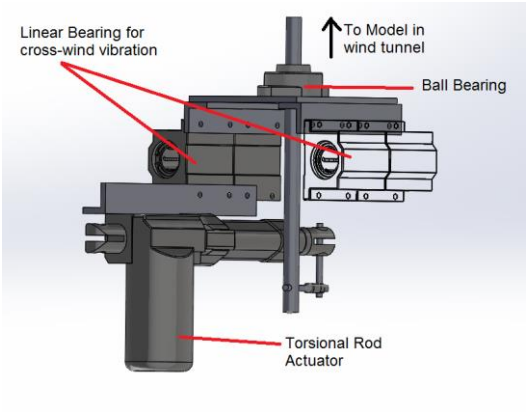


Fig. 4 SolidWorks design interior torsional system mounted on linear bearing for cross-wind vibration

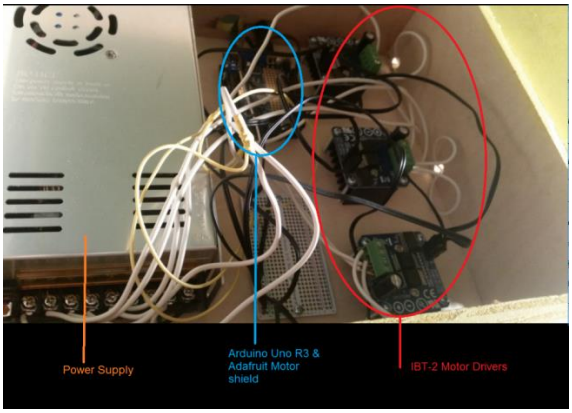


Fig. 5 Interior of control box for the three motors

### *2.4 Wind tunnel used*

The experiments described here were performed in the Aerodynamic and Atmospheric Boundary Layer (AABL) Wind and Gust Tunnel located in the Wind Simulation and Testing Laboratory (WiST Lab) in the Department of Aerospace Engineering at Iowa State University. This wind tunnel has an aerodynamic test section of 2.44 m (8.0 ft) width × 1.83 m (6.0 ft) height, an atmospheric boundary layer test section of 2.44 m (8.0 ft) width × 2.21 m (7.25 ft) height), and a design maximum wind speed of 53 m/s (173.9 ft/s) in the aerodynamic section.

### *2.5 Displacement measurements*

In order to extract the Rational Function Coefficients, it is necessary to measure the displacement of the model and the aerodynamic loads simultaneously. In order to measure the displacements three uniaxial force transducers (*Transducer Techniques*) were connected to the respective relative stationary frame using springs. Each force transducer measured the displacement along one DOF. To ensure that the measurements were correct, they were compared to physical measurements made on the system. Displacement data was captured at 625 Hz using the MATLAB Data Acquisition toolbox.

### *2.6 Aerodynamic load measurements*

All of the section models tested with the system had between 32-42 pressure taps located along their mid-plane. A 64-channel pressure transducer (Scanivalve ZOC33/64 Px) was used to measure the pressures that were later converted to loads on the model. The data was acquired using Scanivalve's Scantel software at a frequency of 312.5 Hz. To ensure the displacement and load time histories were synchronous, a trigger system was used to start both data acquisition systems. All tests were performed in smooth flow (Turbulence Intensity, TI < 0.27%).

## 3. Equations for 3 DOF rational function extraction

For time domain analysis of structures, the equations for the self-excited loads are written first in Laplace domain and then converted to time domain. This method, based on the Rational function formulation (Roger1977, Karpel1982), was developed for two-degrees-of-freedom (vertical and torsional) by (Cao and Sarkar 2012). The Laplace domain formulation is shown in Eq. (1) with expanded terms given in Eq. (2). Eqs. (3)-(5) give the time domain formulation for the self-excited lift, drag and moment after converting from Laplace domain

$$\begin{bmatrix} \hat{L}_{se} \\ \hat{M}_{se} \end{bmatrix} = \underline{V}_f \underline{Q}\underline{\hat{q}} \tag{1}$$

where

$$\underline{V}_f = \begin{bmatrix} \frac{1}{2}\rho U^2 B & 0 & 0 \\ 0 & \frac{1}{2}\rho U^2 B & 0 \\ 0 & 0 & \frac{1}{2}\rho U^2 B^2 \end{bmatrix}, \quad \underline{\hat{q}} = \begin{bmatrix} \hat{h}/B \\ p/B \\ \hat{\alpha} \end{bmatrix}$$

$$\underline{Q} = \begin{bmatrix} (\underline{A}_0)_{11} + (\underline{A}_1)_{11}\, p + \dfrac{(\underline{F})_{11}\, p}{p+\lambda} & (\underline{A}_0)_{12} + (\underline{A}_1)_{12}\, p + \dfrac{(\underline{F})_{12}\, p}{p+\lambda} & (\underline{A}_0)_{13} + (\underline{A}_1)_{13}\, p + \dfrac{(\underline{F})_{13}\, p}{p+\lambda} \\ (\underline{A}_0)_{21} + (\underline{A}_1)_{21}\, p + \dfrac{(\underline{F})_{21}\, p}{p+\lambda} & (\underline{A}_0)_{22} + (\underline{A}_1)_{22}\, p + \dfrac{(\underline{F})_{22}\, p}{p+\lambda} & (\underline{A}_0)_{23} + (\underline{A}_1)_{23}\, p + \dfrac{(\underline{F})_{23}\, p}{p+\lambda} \\ (\underline{A}_0)_{31} + (\underline{A}_1)_{31}\, p + \dfrac{(\underline{F})_{31}\, p}{p+\lambda} & (\underline{A}_0)_{32} + (\underline{A}_1)_{32}\, p + \dfrac{(\underline{F})_{32}\, p}{p+\lambda} & (\underline{A}_0)_{33} + (\underline{A}_1)_{33}\, p + \dfrac{(\underline{F})_{33}\, p}{p+\lambda} \end{bmatrix} \tag{2}$$

$$\begin{aligned} L_{se}(t) = \frac{1}{2}\rho U^2 c\{&((\underline{A}_0)_{11} + (\underline{F})_{11})\frac{h}{c} + (\underline{A}_1)_{11}\frac{\dot{h}}{U} - (\underline{F})_{11}\frac{\lambda_L U}{c^2}\int_0^t e^{-\frac{U}{c}\lambda_L(t-\tau)} h(\tau)d\tau \\ &+((\underline{A}_0)_{12} + (\underline{F})_{12})p + (\underline{A}_1)_{12}\frac{c}{U}\dot{p} - (\underline{F})_{12}\frac{\lambda_L U}{c}\int_0^t e^{-\frac{U}{c}\lambda_L(t-\tau)} p(\tau)d\tau \\ &+((\underline{A}_0)_{13} + (\underline{F})_{13})\alpha + (\underline{A}_1)_{13}\frac{c}{U}\dot{\alpha} - (\underline{F})_{13}\frac{\lambda_L U}{c}\int_0^t e^{-\frac{U}{c}\lambda_L(t-\tau)} \alpha(\tau)d\tau\} \end{aligned} \tag{3}$$

$$\begin{aligned} D_{se}(t) = \frac{1}{2}\rho U^2 c\{&((\underline{A}_0)_{11} + (\underline{F})_{11})\frac{h}{c} + (\underline{A}_1)_{11}\frac{\dot{h}}{U} - (\underline{F})_{11}\frac{\lambda_D U}{c^2}\int_0^t e^{-\frac{U}{c}\lambda_D(t-\tau)} h(\tau)d\tau \\ &+((\underline{A}_0)_{12} + (\underline{F})_{12})p + (\underline{A}_1)_{12}\frac{c}{U}\dot{p} - (\underline{F})_{12}\frac{\lambda_D U}{c}\int_0^t e^{-\frac{U}{c}\lambda_D(t-\tau)} p(\tau)d\tau \\ &+((\underline{A}_0)_{13} + (\underline{F})_{13})\alpha + (\underline{A}_1)_{13}\frac{c}{U}\dot{\alpha} - (\underline{F})_{13}\frac{\lambda_D U}{c}\int_0^t e^{-\frac{U}{c}\lambda_D(t-\tau)} \alpha(\tau)d\tau\} \end{aligned} \tag{4}$$

$$\begin{aligned} M_{se}(t) = \frac{1}{2}\rho U^2 c^2\{&((\underline{A}_0)_{21} + (\underline{F})_{21})\frac{h}{c} + (\underline{A}_1)_{21}\frac{\dot{h}}{U} - (\underline{F})_{21}\frac{\lambda_M U}{c^2}\int_0^t e^{-\frac{U}{c}\lambda_M(t-\tau)} h(\tau)d\tau \\ &+((\underline{A}_0)_{22} + (\underline{F})_{22})p + (\underline{A}_1)_{22}\frac{c}{U}\dot{p} - (\underline{F})_{22}\frac{\lambda_M U}{c}\int_0^t e^{-\frac{U}{c}\lambda_M(t-\tau)} p(\tau)d\tau\} \\ &+((\underline{A}_0)_{23} + (\underline{F})_{23})\alpha + (\underline{A}_1)_{23}\frac{c}{U}\dot{\alpha} - (\underline{F})_{23}\frac{\lambda_M U}{c}\int_0^t e^{-\frac{U}{c}\lambda_M(t-\tau)} \alpha(\tau)d\tau\} \end{aligned} \tag{5}$$

where $\underline{A}_0$, $\underline{A}_1$ are the stiffness matrix and damping matrix, respectively; $\underline{F}$ is the lag matrix, all of order 3 x 3, and $\lambda_L, \lambda_D$ and $\lambda_M$ are the lag coefficients. The elements of $\underline{A}_0$, $\underline{A}_1$ and $\underline{F}$ matrices and $\lambda_L, \lambda_D$ and $\lambda_M$ are known as the Rational function coefficients. *Q*, defined in Eq. (2) is the Rational function matric which contains the 9 Rational functions. In order to validate the extracted Rational function coefficients, it is necessary to convert them to their flutter derivative counterparts. Eq. (6) gives the relationships between the components of the Rational function matrix and the 18 flutter derivatives.

$$
\begin{aligned}
H_1^* &= imag(\underline{Q}_{11})/K^2 & P_1^* &= imag(\underline{Q}_{22})/K^2 & A_1^* &= imag(\underline{Q}_{31})/K^2 \\
H_2^* &= imag(\underline{Q}_{13})/K^2 & P_2^* &= imag(\underline{Q}_{23})/K^2 & A_2^* &= imag(\underline{Q}_{33})/K^2 \\
H_3^* &= real(\underline{Q}_{13})/K^2 & P_3^* &= real(\underline{Q}_{23})/K^2 & A_3^* &= real(\underline{Q}_{33})/K^2 \\
H_4^* &= real(\underline{Q}_{11})/K^2 & P_4^* &= real(\underline{Q}_{22})/K^2 & A_4^* &= real(\underline{Q}_{31})/K^2 \\
H_5^* &= imag(\underline{Q}_{12})/K^2 & P_5^* &= imag(\underline{Q}_{21})/K^2 & A_5^* &= imag(\underline{Q}_{32})/K^2 \\
H_6^* &= real(\underline{Q}_{12})/K^2 & P_6^* &= real(\underline{Q}_{21})/K^2 & A_6^* &= real(\underline{Q}_{32})/K^2
\end{aligned}
\tag{6}
$$

## 4. Experimental set-up, results and discussion

Three section models, a streamlined bridge deck, an asymmetric thick wind turbine blade airfoil, and a rectangular bluff cross section, were used to validate both the three-degree-of-freedom rational function extraction procedure and this system. Each of these models presented a unique case to investigate the applicability of this system. The beauty of this procedure to extract the rational function coefficients for three-degrees-of-freedom is that it requires model tests to be conducted at only three different wind speeds.

### *4.1 Streamlined bridge deck benchmark study*

With the development of longer-span bridges, particularly cable-stayed bridges, the importance of the lateral or along-wind degree-of-freedom on the coupled aeroelastic effects has been emphasized. Further, modern long-span bridges usually use box-girder bridge deck sections with a large aspect ratio (width to depth ratio) making them streamlined that have a better aerodynamic performance. Therefore, a streamlined bridge deck (Fig. 6) was selected for the tests to represent a shallow box girder bridge deck section with semi-circular fairings on the edges. The thickness to chord ratio was 7% and the model was 0.6 m long with a chord length of 0.3 m. This cross section was also chosen because all 18 flutter derivatives of this section had been extracted using a free vibration method (Chowdhury and Sarkar 2004) and the rational functions of this section that are associated with 2 degree-of-freedom (vertical and torsional) were extracted using a forced vibration method (Cao and Sarkar 2012), making it convenient for validation of the current results.

The model was tested at 5 m/s, 6.5 m/s and 9.4 m/s with a forced vibration frequency of 1.06 Hz for all three degrees-of-freedom. The along-wind amplitude ($p$) was 0.1 m (0.5 in), the cross-wind amplitude ($h$) was 0.025 m (1 in), and the torsional amplitude ($\alpha$) was 4 degrees. The results for the rational function coefficients are given below

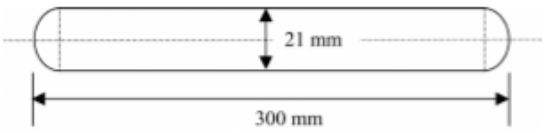


Fig. 6 Cross-section of the streamlined bridge deck

$$A_0 = \begin{bmatrix} 0.737 & 0.067 & -5.185 \\ 0.042 & -0.032 & -0.007 \\ -0.043 & -0.006 & 0.807 \end{bmatrix} \qquad A_1 = \begin{bmatrix} -4.923 & -0.567 & -1.861 \\ 0.720 & -0.886 & -0.109 \\ 1.835 & -0.019 & -0.814 \end{bmatrix}$$

$$F = \begin{bmatrix} -2.421 & -0.013 & 0.651 \\ 0.658 & -0.825 & 0.261 \\ 0.553 & -0.017 & 0.559 \end{bmatrix} \qquad \lambda_L = 0.162;\ \lambda_D = 0.891;\ \lambda_M = 0.2655$$

The rational function coefficients for the 2DOF case (Cao and Sarkar 2012) are copied below

$$\underline{A}_0 = \begin{bmatrix} 0.3273 & -6.2384 \\ -0.0970 & 1.3818 \end{bmatrix},\ \underline{A}_1 = \begin{bmatrix} -3.7549 & -1.4947 \\ 0.8510 & -0.3819 \end{bmatrix},\ \underline{F} = \begin{bmatrix} -0.9484 & 1.3397 \\ 0.2689 & -0.1682 \end{bmatrix},$$

$$\lambda_L = 0.1843,\ \ \lambda_M = 0.2239$$

For further validation, these rational function (RF) coefficients were converted to their flutter derivative counterparts. Fig. 7 shows some selected flutter derivatives for the streamlined bridge deck compared to those extracted from the free vibration test (Chowdhury and Sarkar 2004). These flutter derivatives as converted from RF coefficients using the relationships given in Eqs. (2) and (6) are compared.

### *4.2 Asymmetric wind turbine blade airfoil case*

The National Renewable Energy Laboratory (NREL) has designed a family of S-series airfoils that are thick (high thickness to chord ratio), generate low-noise during operation and aerodynamically efficient with high lift-to-drag ratio, for use in 20-25 m wind turbine blade. A section of the S830 airfoil with a 21% thickness to chord ratio was used for second set of tests.

The airfoil had a chord of 0.15 m (6 in). The maximum lift-to-drag ratio for this airfoil was found to occur at a 6-degree angle of attack, therefore 0, 3, 6, and 9 degree angles of attack were tested. The cross-section of the airfoil is shown in Fig. 8 and an image of the model in the wind tunnel is shown in Fig. 9.

The two degree-of-freedom ($h$, $\alpha$) rational function coefficients for this airfoil as extracted by Sauder and Sarkar (2015) are available for comparison. Also, all 18 flutter derivatives associated with 3DOF for an airfoil NACA0020 that is similar in thickness/chord ratio (20%) to the S830 airfoil (21%) but different from it, as being symmetric, are available for comparison (Chowdhury and Sarkar 2003). The tests for this model were done at 6.5 m/s, 9.4 m/s and 10.9 m/s and frequency of 1.2 Hz. The amplitudes of vibration were h = 38 mm (1.5 in), p = 25 mm (1 in) and α

= 8 degrees. The results for the rational function coefficients of the S830 airfoil at a 0-degree angle of attack are given below and selected flutter derivatives are given in Fig. 10.

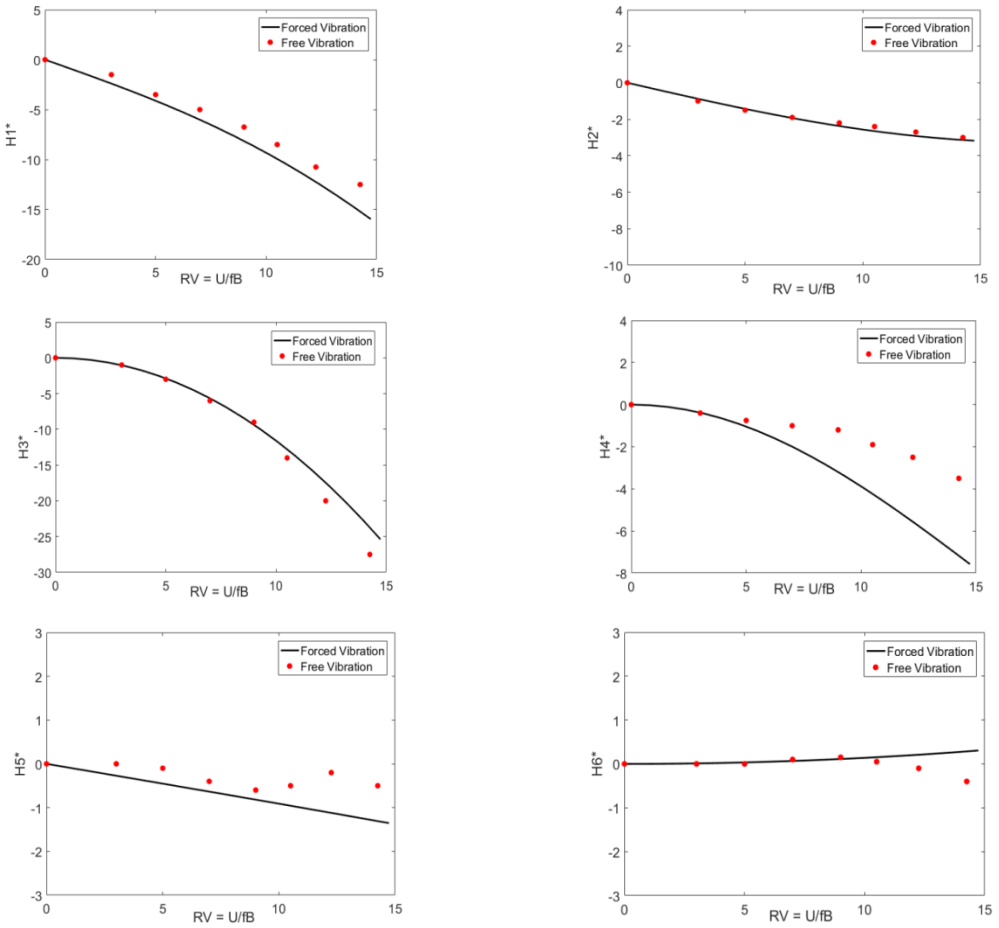


(a)

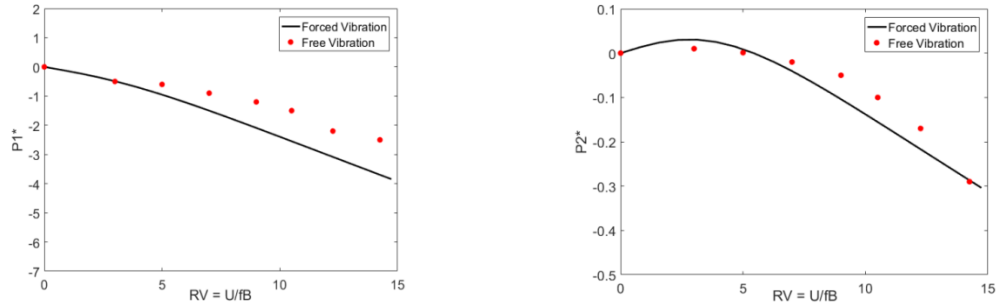


Continued-

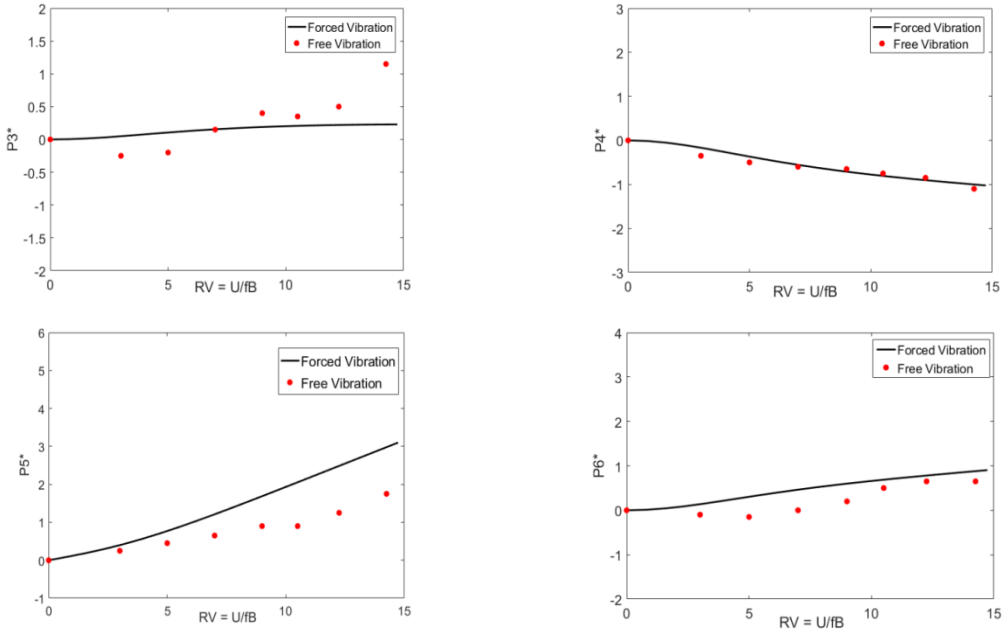
Forced Vibration
Free Vibration
P3*
P4*
P5*
P6*
RV = U/fB

(b)

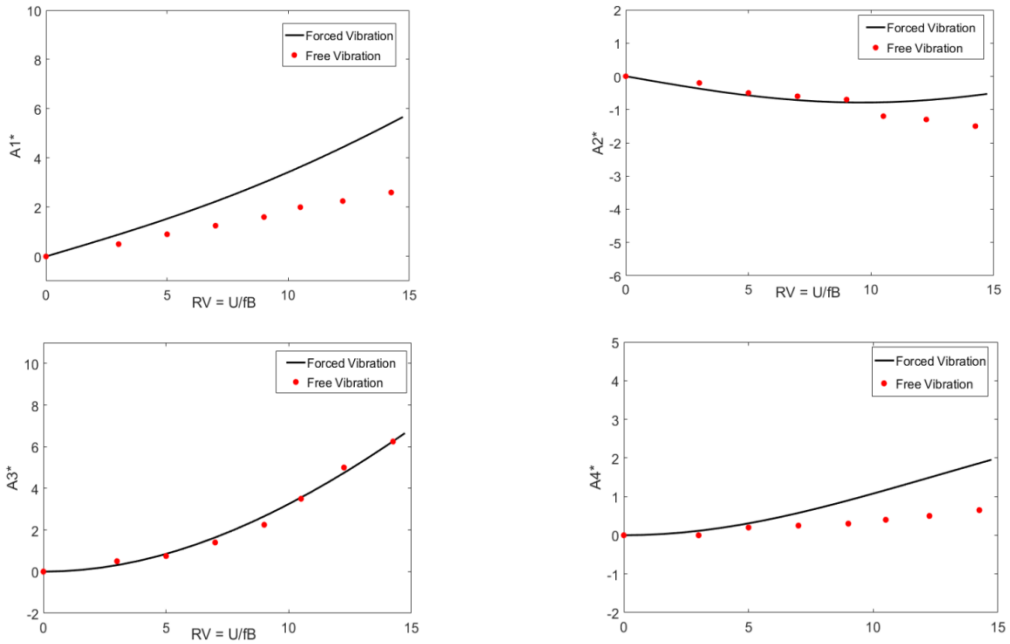
Forced Vibration
Free Vibration
A1*
A2*
A3*
A4*
RV = U/fB

Continued-

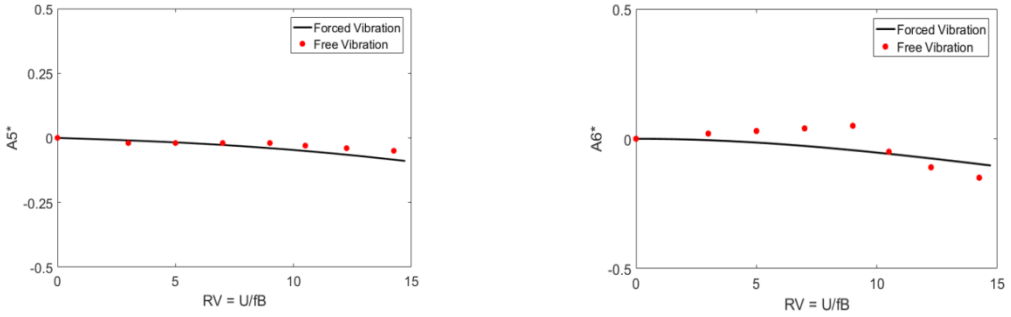


(c)

Fig. 7 Flutter derivatives associated with (a) lift, (b) drag, and (c) moment, for the streamlined bridge deck benchmark study compared to those from free vibration tests (Chowdhury and Sarkar 2004)

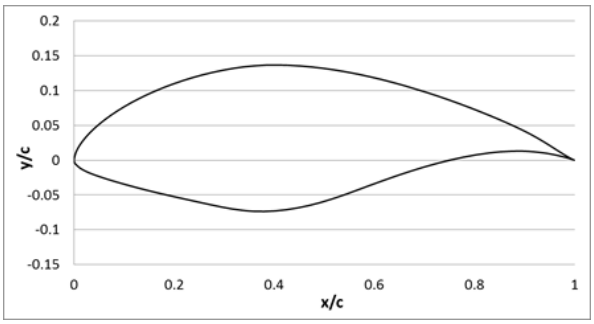


Fig. 8 Profile of the S830 airfoil

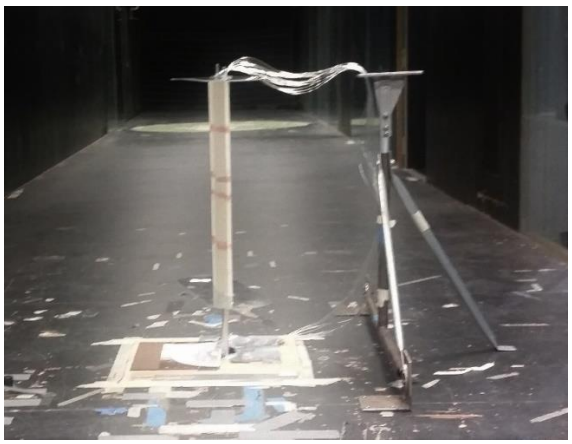

Fig. 9 Airfoil model in wind tunnel as mounted on the 3DOF system (underneath the test section) with a stand for supporting the pressure tubes (upstream view)

$$A_0 = \begin{bmatrix} -1.835 & 0.308 & -2.665 \\ 0.175 & 0.145 & 0.312 \\ 0.828 & -2.312 & -2.405 \end{bmatrix} \qquad A_1 = \begin{bmatrix} -2.969 & -0.379 & -2.195 \\ 0.566 & -0.190 & -0.380 \\ 2.695 & 0.056 & -1.663 \end{bmatrix}$$

$$F = \begin{bmatrix} -2.939 & 0.348 & -0.093 \\ 0.168 & 0.169 & -0.331 \\ -0.497 & 2.420 & 2.476 \end{bmatrix} \qquad \lambda_L = 0.011;\ \lambda_D = 0.016;\ \lambda_M = 0.006$$

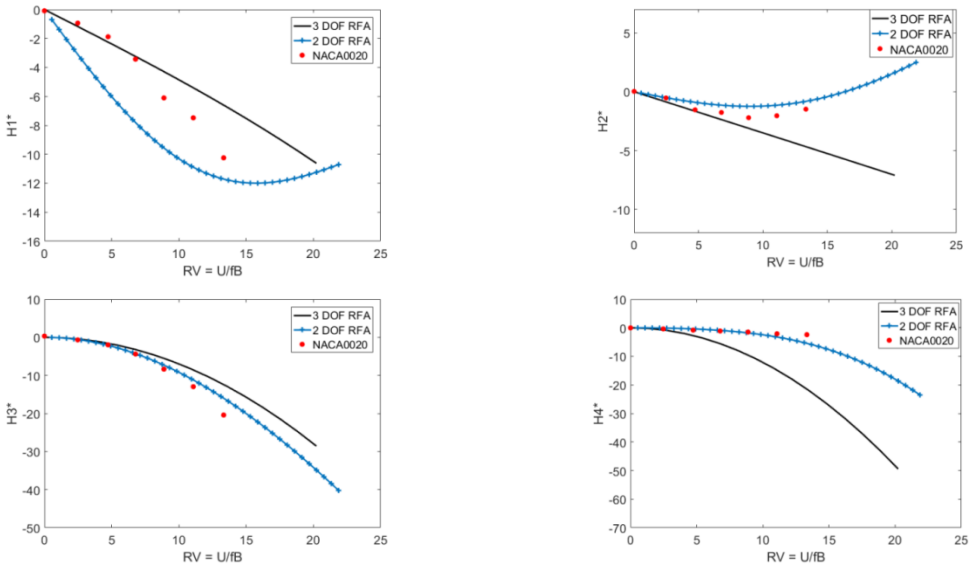


(a)

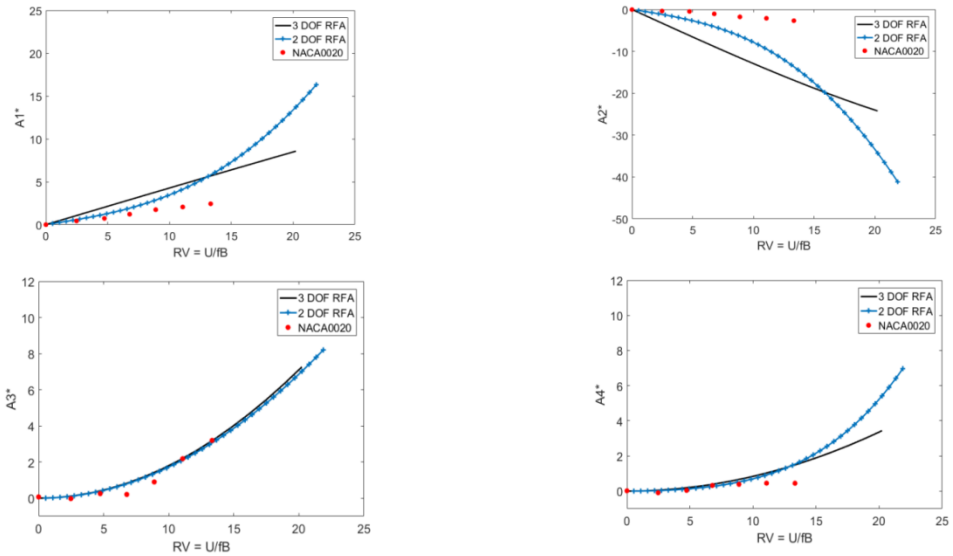


(b)

Fig. 10 Selected flutter derivatives for the S830 airfoil compared to 2 DOF tests (Sauder and Sarkar 2015) and the NACA0020 airfoil (Chowdhury and Sarkar 2003), associated with (a) lift and (b) moment

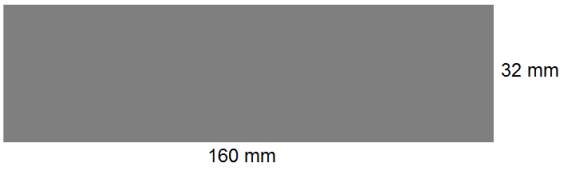


Fig. 11 Cross-section of the bluff rectangular section model

### *4.3 Rectangular bluff cross-section*

To test the robustness of the 3DOF system and the associated method to extract the rational function coefficients for a one-lag load model, it was deemed necessary to test a relatively bluff cross-section of a flexible structure such as a long-span bridge or a tall building. This bluff section model is rectangular with a width-to-depth ratio (B/D) of 5:1, and the length, chord length and thickness of the model are about 0.533 m, 0.16 m, and 0.032 m, respectively (Fig. 11).

The wind speeds used for these tests were 5 m/s, 6.5 m/s and 9.4 m/s with a frequency of 1.06 Hz. The amplitudes of vibration were $h = p$ =12.7 mm (0.5 in), and $\alpha$ = 3 degrees. The extracted rational function coefficients associated with $h$, $p$, $\alpha$ are given below

$$A_0 = \begin{bmatrix} -0.029 & -0.025 & -25.270 \\ -0.017 & -0.014 & -3.567 \\ 0.0627 & -0.049 & -8.747 \end{bmatrix} \qquad A_1 = \begin{bmatrix} -1.672 & -0.836 & 26.166 \\ -2.189 & -0.082 & 29.189 \\ 6.524 & -6.642 & -13.280 \end{bmatrix}$$

$$F = \begin{bmatrix} -13.300 & 0.344 & -16.574 \\ 2.621 & 0.013 & -32.662 \\ -5.048 & -4.636 & 32.452 \end{bmatrix} \quad \lambda_L = 1.225;\ \lambda_D = 1.045;\ \lambda_M = 0.6763$$

For this case the rational function coefficients, as given below, were also extracted using the two degree-of-freedom ($h$, $\alpha$) forced vibration system in a previous study (Cao and Sarkar 2012).

$$\underline{A}_0 = \begin{bmatrix} -0.0618 & -7.9085 \\ -0.0387 & -0.6258 \end{bmatrix},\ \underline{A}_1 = \begin{bmatrix} -0.7820 & 7.3997 \\ -1.7649 & -1.0621 \end{bmatrix},\ \underline{F} = \begin{bmatrix} -10.4613 & -5.7309 \\ -1.5021 & 2.9637 \end{bmatrix},$$

$$\lambda_L = 1.2048,\ \ \lambda_M = 0.7091$$

In this case, only the flutter derivatives determined using a two degree-of-freedom system are available for comparison (Matsumoto *et al*. 1996). Fig. 12 gives the flutter derivatives for the bluff cross-section. A comparison between the 8 flutter derivatives that were determined with the 2 DOF ($h$, $\alpha$) test is presented where applicable. The two results are very similar which suggests that this method can be used for bluff cross-sections as well.

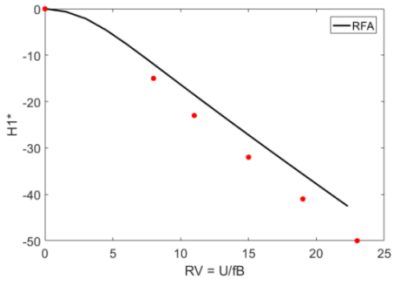
RFA
H1*
RV = U/fB

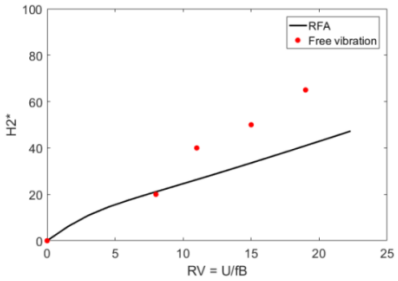
RFA
Free vibration
H2*
RV = U/fB

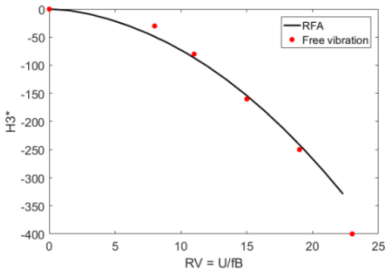
RFA
Free vibration
H3*
RV = U/fB

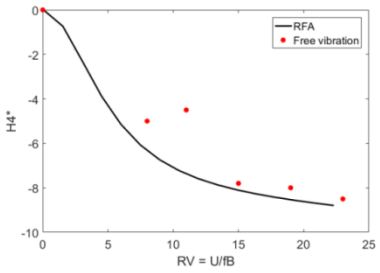
RFA
Free vibration
H4*
RV = U/fB

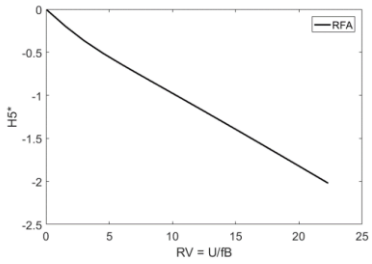
RFA
H5*
RV = U/fB

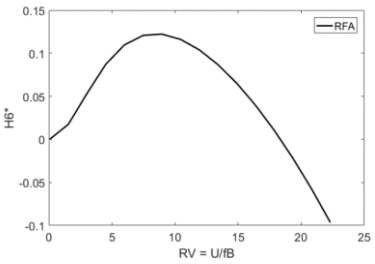
RFA
H6*
RV = U/fB

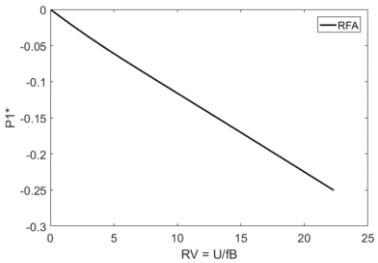
RFA
P1*
RV = U/fB

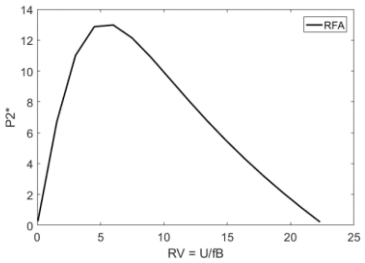
RFA
P2*
RV = U/fB

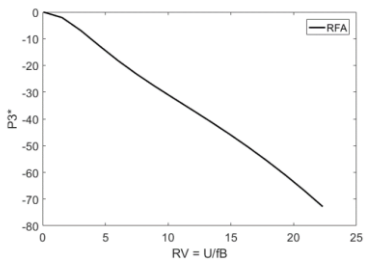
RFA
P3*
RV = U/fB

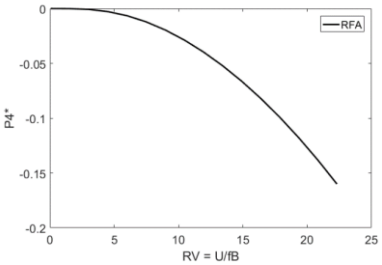
RFA
P4*
RV = U/fB

Continued-

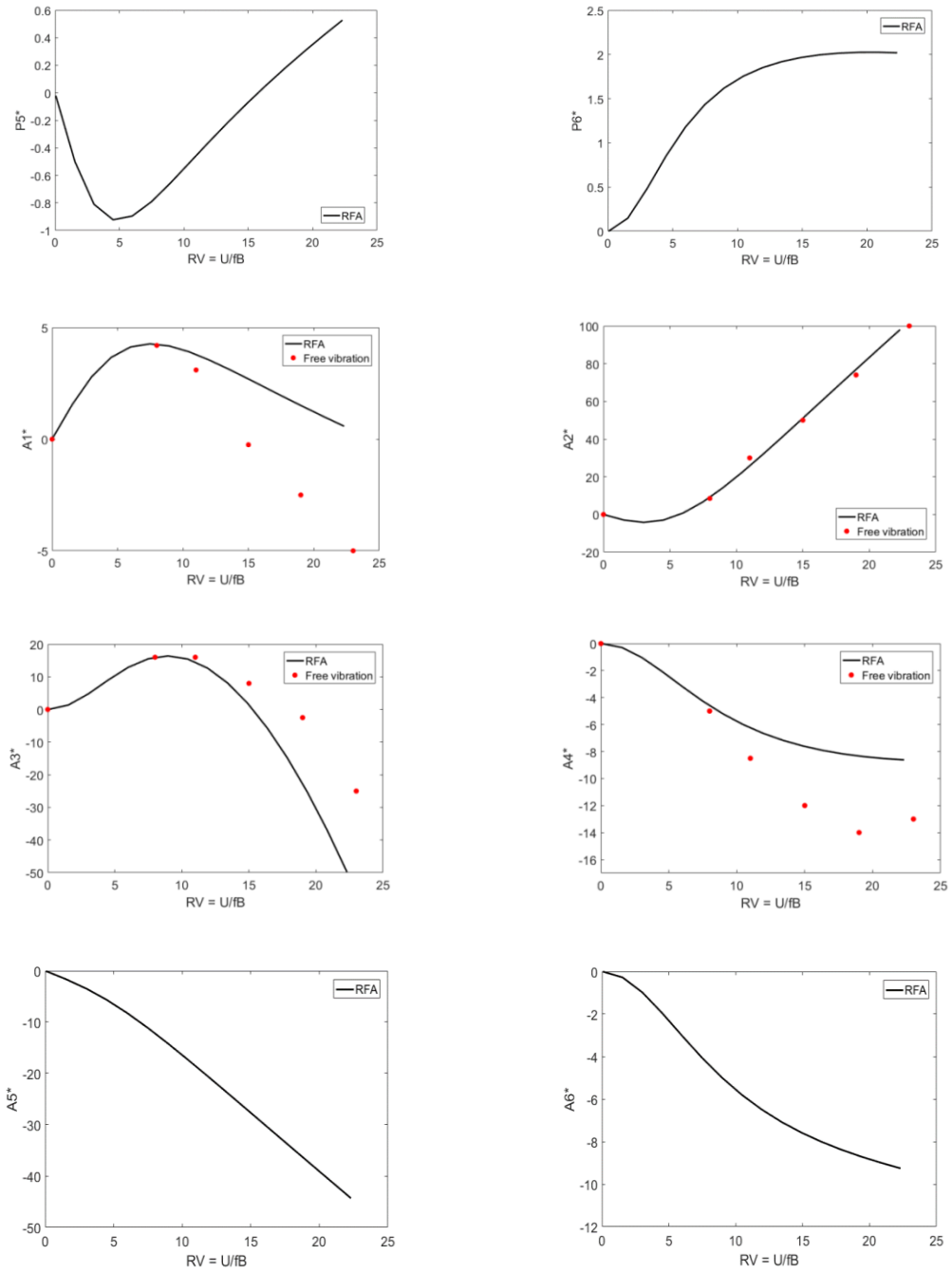


Fig. 12 Comparison of the three degree-of-freedom flutter derivatives for the bluff rectangular cross-section compared to Matsumoto *et al.* (1996) flutter derivatives extracted using two degree-of-freedom (h, α) free vibration

### 4.4 Discussion

In all of the above forced vibration tests, one frequency of vibration was used for all three DOF. Although it is possible to have a unique frequency for each actuator that imparts motion along each DOF, the choice of one frequency for all DOF is because of practical and fundamental considerations. In the past, use of different frequencies along 2-DOF or 3-DOF free vibration section model tests (Sarkar *et al.* 1994, Chowdhury and Sarkar 2004, 2005) to extract flutter derivatives or rational functions have shown that results are independent of the choice of frequency used. The consistency between the flutter derivatives results (Fig. 7) from 3DOF-section model tests of the streamlined bridge deck (Fig. 6) where different frequencies along the 3 DOF were used (Chowdhury and Sarkar 2004) and the current tests where one frequency was used offers further proof of frequency independence.

The discrepancy between some of the flutter derivatives like H1* and A2*, particularly in the higher reduced velocity range, from the current 3DOF tests and past 2DOF results (Sauder and Sarkar 2015) for the airfoil highlights several likely reasons that can improve the outcome of this type of tests in the future. These reasons are (a) possible error in exact resetting of the zero angle of attack for the airfoil model because it was found that the flutter derivatives for this asymmetric and thick airfoil are highly sensitive to the angle of attack; the mechanism to control the torsional motion by a linear actuator in the current setup can be improved by replacing it with a direct motor-driven mechanism that can be better reset, (b) slightly different amplitudes of forced vibration that were used between the 3DOF and 2DOF models; this airfoil because of its asymmetry behaves like a bluff section at zero angle of attack and it is known that flutter derivatives of bluff sections (e.g., rectangular section B/D=2) are highly sensitive to amplitudes; results of comparison between the current 3DOF and 2DOF results from the literature for a bluff, sharp-edged, rectangular cross-section that shows good agreement (Fig. 12) proves the importance of maintaining consistent and low amplitudes of vibration between different tests, (c) higher modes of vibration that occurred (spurious modes) in this setup because this airfoil model was not stiff enough for this 3DOF system setup that uses a cantilevered model; improving the model and setup to avoid this problem is discussed in the next section of the paper, (d) one last reason that is not ruled out completely is the dependence of the aeroleastic loads on the coupled modes; inclusion of the third DOF could influence the aeroelastic load along the other DOFs in some cross sections that are non-symmetric.

## 5. Conclusions

A three degree-of-freedom forced vibration system has been developed that can be used for section model testing in the wind tunnel for simultaneous identification of aeroelastic- damping and stiffness parameters associated with one-, two- and three DOF. This system allows for the simultaneous extraction of all the frequency-domain flutter derivatives or time-domain rational function coefficients and can potentially be used to study other phenomena like vortex shedding and torsional divergence. The functionality and robustness of the system has been successfully demonstrated by testing an asymmetric airfoil used in wind turbine blades, a streamlined bridge deck and a bluff cross-section. Sample flutter derivatives are presented as a means to validate the extracted time-domain rational function coefficients for each cross-section.

While this system worked for the above section models it has some limitations and drawbacks that need to be addressed. First, because the model is cantilevered, it is very easy for the model to experience spurious modes. To avoid that in the presented work, the data was numerically filtered to erase these spurious modes from the data. It should be noted that these additional vibration modes can be mostly avoided by having a stiffer central support bar through the section model that is fixed to the 3DOF system than the ones used in the current models. This could be also corrected by building an additional frame to support the other end of the model so that it is no longer cantilevered.

Overall, this system is able to produce the necessary data to extract the rational function coefficients for all three degrees-of-freedom or any combination of degrees-of-freedom.

## Acknowledgements

The author[a] was supported under the U.S. National Science Foundation Grant No. 1069283 which supports the activities of the Integrative Graduate Education and Research Traineeship (IGERT) in Wind Energy Science, Engineering and Policy (WESEP) at Iowa State University. The authors would also like to acknowledge the support of the undergraduate research assistant, Jonathan Lucktenberg, for his help building this system.

## References

Cao, B. and Sarkar, P.P. (2012), "Identification of rational functions using two-degree-of-freedom model by forced vibration method", *Eng. Struct.*, **43**, 21-30.

Chowdhury, A.G. and Sarkar, P.P. (2003), "A new technique for identification of eighteen flutter derivatives using a three-degree-of-freedom section model", *Eng. Struct.*, **25**, 1763-1772.

Chowdhury, A.G. and Sarkar, P.P. (2004), "Identification of eighteen flutter derivatives of an airfoil and a bridge deck", *Wind Struct.*, **7**(3), 187-202.

Chowdhury, A.G. and Sarkar, P.P. (2005), "Experimental identification of rational function coefficients for time domain flutter analysis," *Engineering Structures, The Journal of Earthquake, Wind and Ocean Engineering*, **27**, 1349-1364.

Dallaire, P.O., Taylor, Z.J. and Stoyanoff S. (2016), "Sectional model tests of tandem bridge decks in dynamic suspension systems", *Proceedings of the 8th International Colloquium on Bluff Body Aerodynamics and Applications*, Boston, MA.

Davenport, A.G. (1962), "Buffeting of a suspension bridge by storm winds", *J. Struct. Eng. - ASCE*, **88**(3), 233-268.

Davenport, A.G., Isyumov, N. and Miyata, T. (1971), "The experimental determination of the response of suspension bridges to turbulent wind", *Proceedings of the 3rd International Conference on Wind Effects on Buildings and Structures*, Tokyo, Japan.

Karpel, M. (1982), "Design for active flutter suppression and gust alleviation using state-space aeroelastic modeling", *J. Aircraft*, **19**(3), 221-227.

Matsumoto, M. (1996), "Aerodynamic damping of prisms", *J. Wind Eng. Ind. Aerod.*, **59**, 159-175

Permata, R., Yonamine, K., Hattori, H. and Shirato, H. (2013), "Aerodynamics and flutter stability of slender bridge deck with double slot and porous cavity", *Proceedings of the 6th Civil Engineering Conference in Asia Region*.

Prud'homme, S., Legeron, F. and Laneville, A. (2015), "Effect of sway movement and motions axis on flutter and vortex induced vibration in a 3 DOF wind tunnel sectional test", *J. Wind Eng. Ind. Aerod.*, **136**,

82-88.
Roger, K. (1977), "Airplane math modeling methods for active control design", AGARD-CP-228.
Sarkar, P.P., Jones, N.P. and Scanlan, R.H. (1994), "Identification of aeroelastic parameters of flexible bridges", *J. Eng. Mech. -ASCE*, **120**(8).
Sarkar, P.P., Gan Chowdhury, A. and Gardner, T.B. (2004), "A novel elastic suspension system for wind tunnel section model studies", *J. Wind Eng. Ind. Aerod*., **92**, 23-40.
Sauder, H.S. and Sarkar, P.P. (2015), "Time-domain aeroelastic loads and response of wind turbine blades", *Proceedings of the 14th Int. Conf. on Wind Eng., Int. Association for Wind Eng.*, Porto Alegre, Brazil, June.
Scanlan, R.H. and Tomko, J.J. (1971), "Airfoil and bridge deck flutter derivatives", *J. Eng. Mech. Div.*, **97**(6), 1717-1733.
Scanlan. R.H., Jones, N.P. and Lorendeaux, O. (1997), "Comparison of taut-strip and section-model-based approaches in long-span bridge aerodynamics", *J. Wind Eng. Ind. Aerod.*, **72**, 275-287.
Scruton, C. (1981), *An Introduction To Wind Effects On Structures*, Oxford University Press, Engineering Design Guides 40.
Strouhal, V. (1878), "On one particular way of tone generation", Annalen der Physik und Chemie (Leipzig), ser. 3.

*AD*